Journal of Theoretical Biology 535 (2022) 110977

Contents lists available at ScienceDirect

Journal of Theoretical Biology

journal homepage: www.elsevier.com/locate/yjtbi

Temporal signaling, population control, and information processing through chromatin-mediated gene regulation

Adi Mukund [a], Lacramioara Bintu [b,*]

[a] Biophysics Program, Stanford University, Stanford, CA 94305, USA
[b] Department of Bioengineering, Stanford University, Stanford, CA 94305, USA

ARTICLE INFO

Article history:
Received 31 August 2021
Revised 3 November 2021
Accepted 5 December 2021
Available online 14 December 2021

Keywords:
Gene regulation
Chromatin
Information theory

ABSTRACT

Chromatin regulation is a key pathway cells use to regulate gene expression in response to temporal stimuli, and is becoming widely used as a platform for synthetic biology applications. Here, we build a mathematical framework for analyzing the response of genetic circuits containing chromatin regulators to temporal signals in mammalian cell populations. Chromatin regulators can silence genes in an all-or-none fashion at the single-cell level, with individual cells stochastically transitioning between active, reversibly silent, and irreversibly silent gene states at constant rates over time. We integrate this mode of regulation with classical gene regulatory motifs, such as autoregulatory and incoherent feedforward loops, to determine the types of responses achievable with duration-dependent signaling. We demonstrate that repressive regulators without long-term epigenetic memory can filter out high frequency noise, and as part of an autoregulatory loop can precisely tune the fraction of cells in a population that expresses a gene of interest. Additionally, we find that repressive regulators with epigenetic memory can sum up and encode the total duration of their recruitment in the fraction of cells irreversibly silenced and, when included in a feed forward loop, enable perfect adaptation. Last, we use an information theoretic approach to show that all-or-none stochastic silencing can be used by populations to transmit information reliably and with high fidelity even in very simple genetic circuits. Altogether, we show that chromatin-mediated gene control enables a repertoire of complex cell population responses to temporal signals and can transmit higher information levels than previously measured in gene regulation.

In mammalian cells genomic DNA is wrapped around histone proteins, forming nucleosomes that assemble into chromatin (Allis and Jenuwein, 2016). Cells use chromatin regulators (CRs) to regulate gene expression; this is a key pathway to coordinate gene expression programs, make and remember decisions, and determine cellular phenotypes (Badeaux and Shi, 2013; Chen and Dent, 2014; Gil and O'Loghlen, 2014; Husmann and Gozani, 2019; Ng and Bird, 2000; Thakore et al., 2016; Valencia and Kadoch, 2019). Recent studies involving site-specific recruitment of repressive chromatin regulators to a reporter gene (Fig. 1A) have shown that they can silence genes in an all-or-none fashion at the single-cell level (Amabile et al., 2016; Bintu et al., 2016; Hathaway et al., 2012). This behavior is useful in situations where responses need to be digital at the level of an individual cell, but where only a fraction of cells in the population need to respond; such scenarios could include regulation of immune signaling (Ng et al., 2018; Tay et al., 2010; Wertek and Xu, 2014), cell differentiation and development (Ferrell and Machleder, 1998), synthetic cell population control (Ma et al., 2020), and apoptosis (Suderman et al., 2017).

The ability to control a cell population in response to temporal signals makes chromatin regulation an attractive platform for engineering novel technologies and therapeutics. In order to fully utilize the potential of chromatin regulation and design new CRs for therapeutic and synthetic biology purposes, we need to understand not only the functional range of CRs, but the theoretical capabilities of CR control.

Traditional control of gene expression in synthetic biology relies on changes to local transcription factor (TF) concentration (Bintu et al., 2005; Garcia et al., 2010; Garcia and Phillips, 2011; Rosenfeld et al., 2002), in which single-cell gene expression levels change proportionally with input signal concentrations (Fig. 1B, left). However, chromatin-mediated all-or-none gene control leads to encoding of signals at the level of populations, wherein the duration of CR recruitment at a target gene determines the fraction of cells with that particular gene silenced (Fig. 1B, right, Bintu et al., 2016). Moreover, many CRs feature long-term epigenetic memory

* Corresponding author.
E-mail addresses: amukund@stanford.edu (A. Mukund), lbintu@stanford.edu (L. Bintu).

https://doi.org/10.1016/j.jtbi.2021.110977
0022-5193/

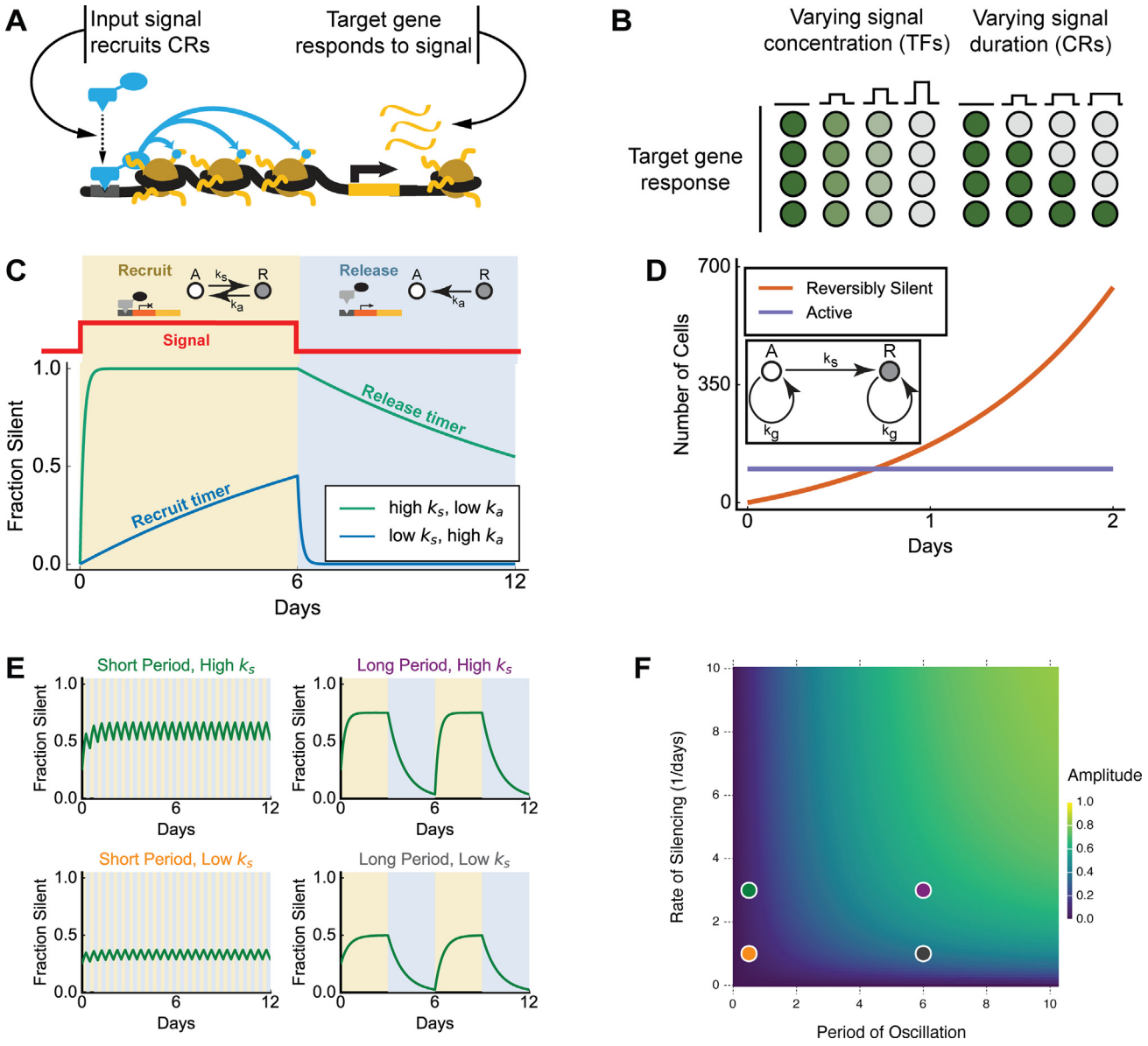

Fig. 1. Memoryless repressive CRs measure the duration of recruitment and filter out noise. A. Input–output relationships for chromatin regulation: input signals can recruit chromatin regulators (CRs) to a target gene (yellow), causing changes in its level of mRNA expression. B. Signals can be modulated in two ways to change gene expression. Left: Increasing the concentration of a transcription factor (increasing height of step signal) causes gene expression changes in all cells in the population (column) in a graded manner from high (green) to low (gray). Right: Increasing the duration of recruitment of a CR (increasing width of step signal), causing all-or-none single-cell responses (green to gray) with a different fraction of the population responding to each duration (columns). C. Two-state model for reversible gene silencing and reactivation. Top left: a repressive chromatin regulator is recruited at a target gene that starts active (A), and induces its transition to a reversibly silent state R with a rate k_s. Top right: upon release of the CR, the gene reactivates at a rate k_a. Bottom: the fraction of cells silent is plotted during recruitment and release of 2 chromatin regulators: blue with $k_s = 0.1$/day and $k_a = 10$/day, and green with $k_s = 10$/day and $k_a = 0.1$/day. D. Number of cells active (purple) and silent (orange) over time during recruitment of a silencing CR with $k_s = 1$/day and $k_a = 0$/day for a population that starts with 100 cells, all of them active, and grows at a rate $k_g = 1$/day. Inset: kinetic scheme describing population growth and silencing. E. Fraction of cells silent in response to pulsatile recruitment of a CR. Periods of recruitment (shaded yellow) and release (shaded blue) are equal to each other and set to 0.25 days (left, short) or 3 days (right, long). The CRs recruited have $k_s = 3$/day (high, top) or $k_s = 1$/day (low, bottom). F. Amplitude of response to oscillations (expressed as fraction of cells silent) as a function of the period of oscillation and silencing rate (k_s) when $k_a = 1$/day. Colored dots correspond to plots in panel E, where the color of the title in panel E is the same as the corresponding dots.

in which a well-controlled fraction of cells remains silent indefinitely after release of the chromatin regulator.

This all-or-none single-cell behavior and fractional population response characteristic of CRs can be described via a phenomenological model in which cells stochastically transition between active and silent expression states (Bintu et al., 2016; Hathaway et al., 2012). Here, we use this model to show examples of gene expression control achievable by chromatin regulators with different rates of silencing and degrees of epigenetic memory. We first demonstrate the utility of CRs in filtering out noise and maintaining either a constant number or constant fraction of cells in a particular state in a population. We then show that chromatin regulators that feature long-term epigenetic memory serve as timers that measure the total duration of recruitment via the irreversibly silenced fraction of cells. We show that using activating and repressor CRs together enables the construction of complex behaviors such as adaptation. Last, we quantify the ability of CRs to transmit signals through epigenetic signaling circuits and find that population-level responses to CR signaling allow for more information transmission than single-cell changes to gene expres-

sion. Together, these results provide the mathematical framework necessary to analyze naturally occurring genetic circuits that contain chromatin regulators and design novel mammalian synthetic circuits that incorporate temporal control at the level of the cell population.

1. Chromatin regulators without memory enable population stopwatches and set-point control

Chromatin regulators without long-term memory reversibly silence genes in an all-or-none fashion, with the fraction of cells silent in a population depending on the duration of CR recruitment. This behavior can be captured via a two-state phenomenological model in which cells are either active or reversibly silent. During CR recruitment, cells transition from the active to reversibly silent state at a rate k_s and back at a rate k_a. After CR release, reversibly silent cells reactivate with rate k_a (Fig. 1C, top). This produces an exponential increase in the fraction of silent cells during recruitment, followed by an exponential decay during release Supplementary Information. During recruitment, the fraction of silent cells serves as a direct measure of the duration of CR recruitment so far (Fig. 1C, left). Release allows the system to reset itself and can also measure the duration since the end of recruitment if the system starts with all cells silent (Fig. 1C, right). For example, a chromatin regulator with slow silencing (low k_s) and fast reactivation (high k_a) will be able to measure time throughout a recruitment period (Fig. 1C, blue curve) while a chromatin regulator with fast silencing (high k_s) and slow reactivation (low k_a) will measure time throughout release (Fig. 1C, green curve). The rate of silencing for a given chromatin regulator determines the timespan during which the response to increasing recruitment duration is linear. In this regime, if reactivation rates are small compared to silencing rates, the change in fraction of cells silent (R) is linear with recruitment time ($\Delta R_{recruit} \approx k_s \Delta t$, Fig. 1C blue curve). Similarly, during the release period, the decrease in silent cells can be made linearly proportional to the time since the end of recruitment ($\Delta R_{release} \approx -k_a \Delta \tau$). In practice, k_s and k_a can be tuned by changing the number or strength of binding sites for the chromatin regulator at the target gene, or by changing the type of regulators recruited (Bintu et al., 2016).

Interestingly, coupling the rate at which a CR silences a target gene to the rate of population growth allows one to maintain a constant total number of active cells in the population. In conditions where: (1) active cells divide to produce 2 active daughter cells and silent cells divide to produce 2 silent daughter cells, and (2) a repressive CR is continually recruited to its target in all cells, setting the rate of target gene silencing to be equal to the rate of population growth allows for the maintenance of a constant number of active cells (Fig. 1D). This can be easily seen when examining the differential equation governing the dynamics of such a scenario. If the number of active cells is denoted as N_A, the rate of target gene silencing is denoted as k_s, and the rate of population growth is denoted as k_g, then $\frac{dN_A}{dt} = N_A(k_g - k_s)$. In turn, setting $k_g = k_s$ gives $\frac{dN_A}{dt} = 0$, meaning that the number of active cells will remain constant over time while the number of silent cells will grow exponentially. This is a simple mechanism for creating a cell niche, in which a constant number of cells in a population can be kept exhibiting a phenotype such as stemness. Moreover, if the expression of the active gene is coupled to a survival mechanism (such as antibiotic selection), and all cells that silence it can be easily killed, one could create a self-renewing population of constant size.

Up until this point we have only considered continuous stretches of CR recruitment to a target gene; however, discontinuous pulsatile recruitment that drives oscillatory behavior is a widespread pattern in cell signaling (Dalal et al., 2014; Levine et al., 2012; Levine et al., 2013; Lin et al., 2015). Pulsatile recruitment of CRs produces oscillatory population responses whose frequency can be tuned by varying the duration of CR recruitment pulses and the gaps between them (Fig. 1E, left vs right). Varying the duration of pulsing changes not only the frequency of the target gene oscillations, but also their amplitude: with less time for silencing and reactivation, fewer cells can transition from active to silent. Notably, recruitment pulses with relatively high frequencies (i.e. short pulse durations) produce oscillations with relatively small amplitudes (Fig. 1E, left); the threshold at which the amplitudes become undetectably small is determined by the k_s of the CR (blue region of Fig. 1F). In other words, these faster fluctuations are filtered out from affecting downstream gene expression. Tuning the k_s of the CR determines the threshold frequency at which potentially noisy fluctuations in CR binding are filtered out. CRs with silencing rates in the range of experimentally measured values (Bintu et al., 2016) can filter out noise with a period less than one day, but mediate a strong response for longer periods of signal on the order of days; such signals could include circadian oscillations (Levine et al., 2013) or cold-induced plant vernalization (Song et al., 2012).

Autoregulation, in which a transcription factor regulates its own expression, is a key motif in signal transduction pathways (Alon, 2019). Autoregulatory loops can ensure a constant level of output despite varying levels of input to a circuit. Developmental programs frequently use autoregulatory motifs to tightly control protein levels throughout differentiation (Crews and Pearson, 2009). We wondered whether a memoryless CR that represses its own expression (Fig. 2A) could generate a population with a fixed fraction of active cells. We began with a simplified model, where we assume that the levels of CR change instantaneously in response to changes in gene activity. For any given cell expressing the CR, the rate of silencing of the gene expressing the CR is simply the k_s associated with that CR. If the cell does not express the CR, the rate of silencing is 0 and the rate of reactivation is k_a. Because the fraction of cells with the CR-encoding gene active (A) and the fraction silent (R) need to add up to 1, the active fraction can be described as:

$$\frac{dA}{dt} = -k_s A + k_a(1 - A) \tag{1}$$

Regardless of the starting point, the fraction of active cells eventually converges to a fixed point determined by the k_s and k_a values of the autoregulating CR (Fig. 2B). The value of the steady state fraction of cells with the gene expressing the CR being active can be computed analytically as $A_{ss} = k_a/(k_a + k_s)$, and thus can be thought of as a function of the k_s/k_a ratio (Fig. 2C). This ratio and the rates of silencing and reactivation depend on the chromatin regulator, the promoter, the genomic locus and cell type.

This simple model does not account for the fact that it can take some time for the CR to change at the protein level after its encoding gene changes states: the CR can still be present in a cell even when its corresponding gene is not actively being transcribed. Importantly, the kinetics of both promoter activity and protein degradation can significantly change the overall dynamics of gene expression (Al-Radhawi et al., 2019). Measured rates of protein degradation range from nearly 0 for very stable proteins to over 100/day (Doherty et al., 2009). To account for protein production and degradation rates, we considered a stochastic model in which a promoter in a given cell can transition between active and reversibly silent states (as before), and proteins are produced during the active state and can be degraded at all times (Fig. 2D). We also assumed that the rate of gene silencing is a Hill function with respect to the concentration of CR in that cell (Fig. 2E, Supplementary Information). We performed stochastic simulations of a population of cells undergoing CR autoregulation using this model

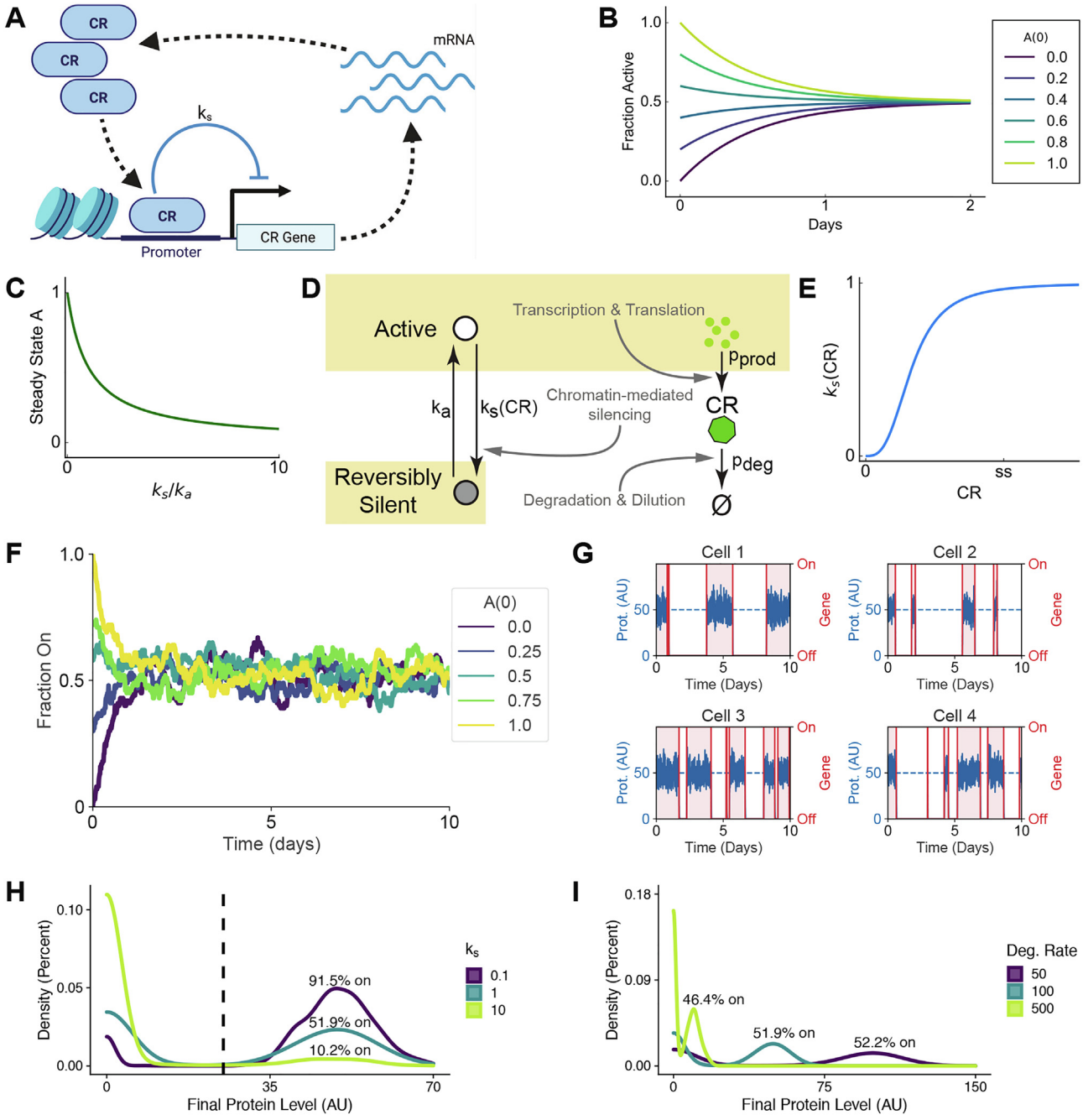

Fig. 2. Autoregulation of a repressive CR stabilizes the fraction of active cells in a population. A. Schematic for CR autoregulation: a CR is transcribed into mRNA and translated into protein, and represses its own gene. B. Fraction of cells expressing a CR (with $k_a = 1/\text{day}$ and $k_s = 1/\text{day}$) as a function of time after beginning with varying fractions of active cells. C. Steady-state fraction of active cells for a population in which a CR represses itself as a function of the k_s/k_a ratio for that CR. D. Stochastic model for CR regulation involves chromatin-mediated gene silencing, protein production via transcription and translation, and protein loss via degradation and dilution. E. The silencing rate k_s as a function of CR protein concentration in each cell $[CR]$ is defined as $k_s = k_{s\ max}\frac{[CR]^3}{[CR]^3+\left([CR]_{max}/3\right)^3}$ where $[CR]_{max} = \frac{p_{prod}}{p_{deg}}$ is the ratio of the protein production and degradation rates, and $k_{s\ max}$ is the maximum silencing rate achievable by this CR (**Supplementary Information**). F. Fraction of cells expressing a CR with $k_a = 1/\text{day}, k_{s\ max} = 1/\text{day}, p_{prod} = 5000/\text{day}, p_{deg} = 100/\text{day}$ over a period of 10 days, with $A(0) \in \{0.00, 0.25, 0.50, 0.75, 1.00\}$ being the initial fraction of cells initialized with active promoter states. G. Representative simulated single-cell traces showing the level of protein (cyan) and gene promoter status (red) for a range of protein degradation and silencing rates for an autoregulating CR with $k_a = 1/\text{day}, k_{s\ max} = 1/\text{day}, p_{prod} = 5000/\text{day}, p_{deg} = 100/\text{day}$. Horizontal lines indicate the steady-state ON level of protein, i.e. production rate/degradation rate. H. Probability density of final levels of CR protein in cells when protein degradation is high: $k_a = 1/\text{day}, p_{prod} = 5000/\text{day}, p_{deg} = 100/\text{day}$, shown for three different values levels of $k_{s\ max}$. Percentage of cells with high levels of CR is computed as the proportion of cells with protein values higher than half of the steady state value in the absence of feedback ($[CR] \geqslant 0.5 \cdot p_{prod}/p_{deg}$ at the end of the simulation, vertical dashed line). I. Probability density plot of final levels of CR protein in cells expressing a CR with $k_a = 1/\text{day}, k_{s\ max} = 1/\text{day}, p_{prod} = 5000/\text{day}$ for three different values of protein degradation rate p_{deg}. Percentage of cells with high levels of CR is computed as the proportion of cells with $[CR] \geqslant 0.5 \cdot p_{prod}/p_{deg}$ at the end of the simulation.

(Supplementary Information), and found that the steady-state fraction of cells with an active promoter in the population remained the same across a range of protein production (p_{prod}) and degradation (p_{deg}) rates, as expected (Figure S1A). Also as expected, increasing the value of k_s reduced the duration of time an individual cell's promoter was actively expressing the gene, while

increasing the protein degradation rate reduced the level of protein in individual cells while the gene was active (Figure S1B). Encouragingly, we found that the results from the stochastic model matched predictions made using the simpler phenomenological model (Fig. 2F), and were able to observe individual cells producing and degrading protein while transitioning between active and silent promoter states at rates matching our predictions (Fig. 2G).

In regimes of fast protein degradation compared to silencing and reactivation (i.e. high p_{deg}) increasing the silencing rate k_s while holding the overall CR degradation constant decreased the steady state fraction of cells with high CR protein expression (denoted *High* from here on) without altering the level of steady state protein in these active cells (Fig. 2H). Increasing the rate of the CR degradation rate (p_{deg}) while holding the maximum silencing rate constant (Supplementary Information) decreases the level of protein in the *High* cells, but does not alter the fraction of cells with high levels of CR protein too much (Fig. 2I). Thus, at high degradation rates autoregulatory CR loops allow for orthogonal manipulation of protein levels in individual cells and the fraction of cells with high expression in an entire population.

However, in regimes of slow protein degradation (i.e. low p_{deg}), varying the silencing rate k_s simultaneously changes the fraction of cells in the *High* CR expression state and the level of protein in *High* cells (Figure S1C). Additionally, low degradation rates produced unimodal distributions of protein levels with broad peaks, as opposed to the sharp peaks and bimodal distributions of high degradation rate regimes (Figure S1C, S1D). These distributions correspond to a broad sampling of all expression levels of a particular protein throughout a population. Such an expression profile allows for bet hedging, in which the population can mitigate risks related to a changing environment by diversifying the set of phenotypes expressed by its constituent cells (Fraser and Kaern, 2009; Shaffer et al., 2017).

2. Chromatin regulators with epigenetic memory act as time integrators

One of the more remarkable features of chromatin regulators is their ability to silence genes permanently, such that cells remain silent for an indefinite period of time after release. CRs associated with histone methylation, such as members of the Polycomb and HP1 pathways, were shown to silence a large number of cells upon recruitment, with only a fraction of cells reactivating upon release (Bintu et al., 2016). This type of fractional epigenetic memory may prove crucial in scenarios where an acute phase response needs to be significantly stronger than a nonzero long-term response. For example, such signals can be useful during embryological development, when a large amount of cell proliferation is necessary in the acute phase for morphogenesis, but a small amount of long-term proliferation is also needed for maintenance of healthy organs (Nguyen et al., 2018).

We have previously described CRs with memory via a three-state model in which cells transition between active, reversibly silent, and irreversibly silent states with rates that vary based upon the recruited CR. During recruitment, cells transition from the active to reversibly silent state at rate k_s, from the reversibly silent to the irreversibly silent state at rate k_i, and from the reversibly silent to the active state at rate k_a; during release, cells in the reversibly silent state transition to the active state at rate k_a (Fig. 3A). The fraction of cells in each state as a function of time can be solved analytically from the differential equations associated with the transition rates (Bintu et al., 2016) (Fig. 3A, Supplementary Information). These equations accurately describe the dynamics of the population only when protein production/degradation rates are high in comparison to rates of gene silencing/reactivation, and the population of cells is bimodal such that cells with active promoters are clearly separable from cells with silent promoters despite single-cell heterogeneity. Sampling the parameter space of these rates shows that chromatin regulation can achieve a wide range of population-level dynamics (Figure S2A, S2B).

Chromatin repressors with memory can act as timers that integrate the total duration of a signal, even when this signal is not continuous in time. We plotted the fraction of cells in the three states during and after a series of 5 one-day pulses of recruitment separated by one-day release periods for the CR initially considered in Fig. 3A. With these parameters the fraction of irreversibly silent cells rose linearly during periods of recruitment and remained flat during periods of release (Fig. 3B), consistent with previous observations that the fraction of irreversibly silent cells measures the total duration of recruitment (Bintu et al., 2016). Comparing the fraction of irreversibly silenced cells between pulsatile and non-pulsatile recruitment modes revealed only a small difference in the total number of irreversibly silent cells at the end of recruitment between the two modes (Fig. 3C). However, we found that choosing other parameters for the CR with memory (Figure S2C) allowed us to generate visible differences between pulsatile and continuous recruitment (Figure S2D).

We decided to compute an upper bound on the difference between the irreversibly silent fractions associated with continuous versus pulsatile recruitment.To do so, we considered a simple scenario in which recruitment was either done for 2 continuous days, or as two separate 1 day pulses with a gap in the middle. At the end of the first day of recruitment, both regimes must feature the same number of irreversibly silent cells. However, the periods of CR release in the pulsed regime cause some of the reversibly off cells to become active; this shift does not happen in the continuous recruitment regime. Thus, any gap in the fraction of irreversibly silent cells when comparing pulsed versus non-pulsed recruitment must be due to this difference in the number of reversibly silent cells at the beginning of the second day of recruitment. We produced an upper bound on this gap by computing the fraction irreversibly silenced during any single pulse if the entire population starts active, and comparing that to the fraction irreversibly silenced if the entire population starts reversibly silent. We were able to derive an expression for the pulse length at which the two fractions would be maximally different, and thus an expression for the maximum possible gap between the two fractions of irreversibly silenced cells (Supplementary Information). We found that for CRs with high rates of silencing compared to commitment to the irreversible state (i.e. $k_s \gg k_i$), the maximum gap is quite small and thus pulsing produces the same outcome as continuous recruitment (Figure S2E).

3. A chromatin-based feed-forward loop for perfect adaptation

While up until this point we primarily examined behaviors that can be produced using a single CR, we ultimately wanted to be able to reproduce signal transduction behavioral motifs using multiple CRs. We chose to focus on adaptation as a complex behavior that would require interactions between multiple CRs in a single circuit. While traditional genetic circuits producing adaptation operate at the level of individual cells, we wanted to produce adaptation on the level of whole populations, where instead of controlling the abundance of a protein in a cell we would control the abundance of a phenotype in a population. To build a circuit exhibiting adaptive behavior, we needed CR activators as well as CR repressors. Activators can be thought of as the mirror images of reversible repressors: stochastic, all-or-none genetic devices that can activate a reversibly silenced gene at rate k_p. In its absence, the gene can background silence at rate k_r (Fig. 3D).

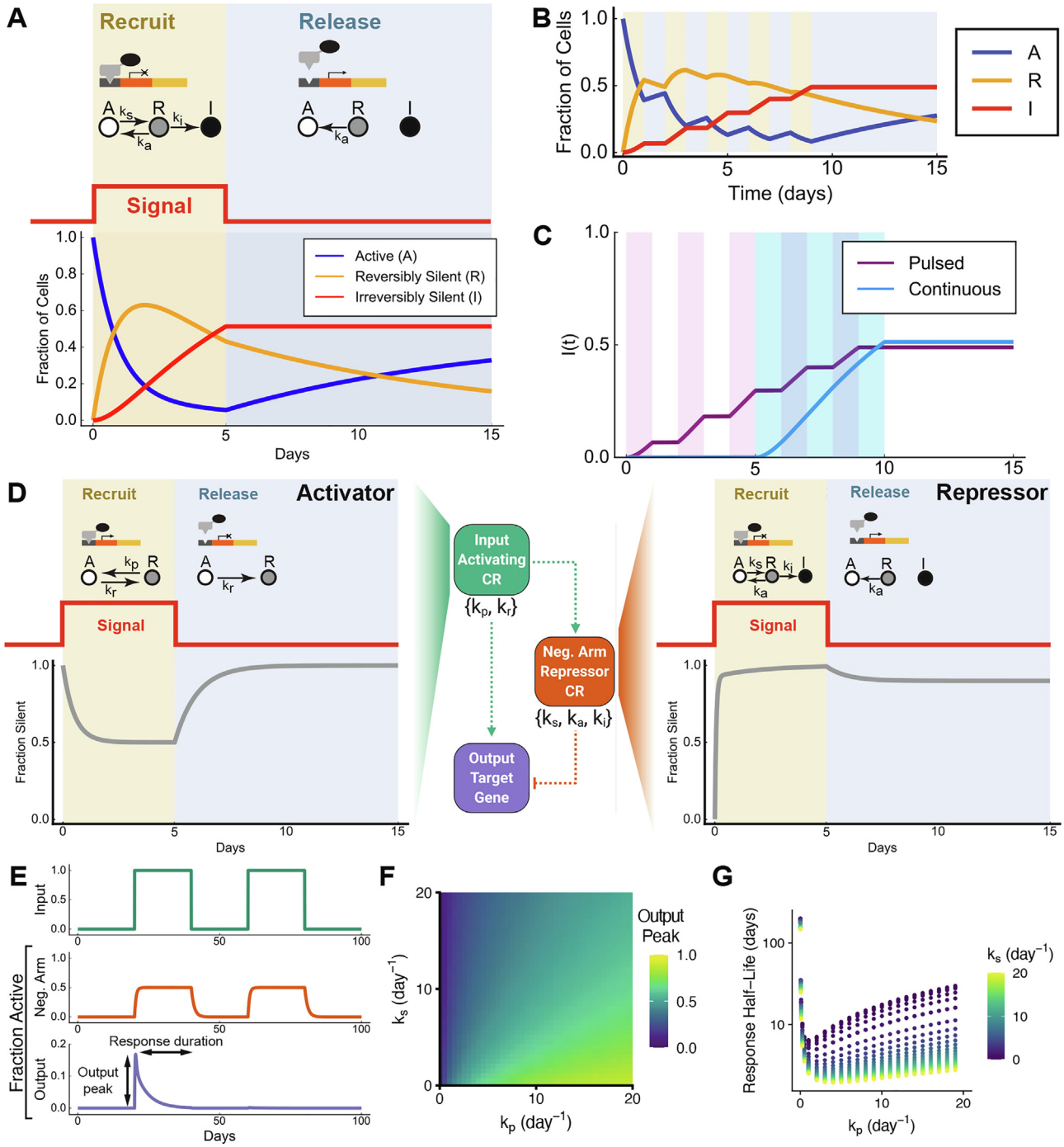

Fig. 3. Chromatin regulators with epigenetic memory act as molecular timers and can be used to generate perfect adaptation via incoherent feedforward loops. A. Three-state model for reversible and irreversible gene silencing and reactivation along with dynamics of silencing and reactivation for a CR with $k_s = 1/\text{day}, k_i = 0.2/\text{day}$ and $k_a = 0.1/\text{day}$. B. Dynamics of silencing and reactivation during pulsatile recruitment of the CR with rates used in panel A. Shaded regions indicate times where the CR is recruited to the gene. 'A' refers to active cells, 'R' to reversibly silent cells, and 'I' to irreversibly silent cells. C. Fraction of cells irreversibly silenced when the CR with rates as in panel A&B is recruited in a pulsatile manner (purple) compared with continuous recruitment for the same total duration (cyan). D. Schematic of an incoherent feedforward loop. Center: The input consists of recruitment of a CR that activates in an all-or-none manner both the output target gene and a gene encoding for a repressor CR of the output gene. Left: two-state model and dynamics of an input activator with $k_p = 1/\text{day}, k_r = 1/\text{day}$. Right: three-state model and dynamics of an input silencer with memory with $k_s = 15/\text{day}, k_a = 0.1/\text{day}, k_i = 0.5/\text{day}$. E. Dynamics of the fraction of cells that activate the repressor (orange) and output gene (purple) in response to two pulses in the input signal (activator recruitment, green) for the incoherent feedforward system described in A. F. Peak of the first output response as a function of the input CR's activation rate (k_p) and the repressor CR's silencing rate (k_s), for $k_r = 0, k_a = 0.1/\text{day}$ and $k_i = 0.5/\text{day}$. G. Half-life of the first output response as a function of the input CR's rate of activation (k_p), with the rate of repressor silencing indicated by the color of each point. Here, k_i was chosen to be 0.5/day and k_a was chosen to be 0.1/day .

Incoherent feedforward loops provide an efficient mechanism for generating adaptive behaviors in signal transduction pathways (Bleris et al., 2011). These loops are frequently seen in the context of nuclear receptors that control responses to estrogens, progestins, glucocorticoids, and other ligands, as transcription factors are often the targets of these various loops (Sasse and Gerber, 2015). While there are other mechanisms for generating adaptation, including interlinked positive and negative feedback loops

(Ferrell, 2016), we chose to focus on the incoherent feedforward motif as a simple motif that could still exhibit sophisticated behavior. This motif consists of an activator CR acting both on a target output gene and on a gene encoding for a repressor of the output gene (Fig. 3D, center). Thus, an initial stimulus first activates the target, and the activation of the repressor causes the target to return to baseline. Using a repressor with epigenetic memory causes the target gene to be converted to an irreversibly silent state in which it can no longer respond to a second stimulus (Fig. 3E).

We were interested in understanding how the dynamics of the activating and repressor CRs involved in such an incoherent feedforward loop affect the magnitude of the initial response to an activating stimulus, as well as the half-life of the decay process after the peak. Increasing the silencing rate (k_s) of the repressor CR reduces the output peak (Fig. 3F) and the output half life (Figure S2F). In contrast, increasing the activation rate of the activator CR (k_p) increased the magnitude of the output (Figure S2G) while also increasing the output half-life (Fig. 3G). Our initial parameter choices produced a system with no responses to further stimulation after the first peak. However, this is not always the case: decreasing either the k_s or the k_i of the repressor increased the magnitude of the secondary response (Figure S2H). This is because reducing the rate at which cells are converted to irreversibly silent increases the population of cells that can reactivate and be used for further responses.

4. Information transmission via all-or-none chromatin regulation

CRs with memory can be used to generate complex behavior such as time integration and perfect adaptation, suggesting that CRs with memory could encode more information than memoryless CRs. In order to quantify the information content associated with each CR, we used an information theory-based approach that has been used in the past (Cheong et al., 2011; Lee et al., 2021; Selimkhanov et al., 2014; Suderman et al., 2017) and applied it to previously published experimental data (Bintu et al., 2016).

The information carried by a signaling channel can be quantified by representing the input signal as a random variable X and the output signal as a random variable Y, and then computing the mutual information between X and Y (MacKay and Mac, 2003):

$$I(X,Y) = \int_{x\in X}\int_{y\in Y} p(x,y)\log_2\left(\frac{p(x,y)}{p_X(x)p_Y(y)}\right) \quad (2)$$

The units of information are determined by the base of the logarithm; the typical choice of base 2 quantifies information in bits. While the distribution of Y is totally determined by the signaling channel, the distribution of X is variable, and changing this input distribution changes the amount of information carried by the channel (Fig. 4A). The channel capacity C is defined as the maximum possible value of $I(X,Y)$ over all possible input distributions, and represents the maximum amount of information that the signaling channel can transmit. This approach provides a generalizable measure of the signaling potential of different channels, enabling comparisons of the signaling capacity of chromatin regulation with the capacities of other well-known cellular signaling pathways (Komorowski and Tawfik, 2019; Razo-Mejia et al., 2020; Uda et al., 2013; Uda and Kuroda, 2016). Alternately stated, the channel capacity of a pathway quantifies in bits the ability of the output of a signaling channel to allow a receiver to distinguish between different inputs (Shannon, 1948). Channels with higher capacities are capable of transmitting greater information than channels with lower capacities. For example, a channel capacity of 1 bit corresponds to a signal that can distinguish between 2 distinct inputs, a channel capacity of 2 bits corresponds to a signal that can distinguish between 4 distinct outputs, and so on.

Since single-cell responses to CR recruitment are inherently stochastic, we were interested in comparing the single-cell and population-level signaling channels for different CRs. We began by computing an experimental channel capacity based on previously published data (Bintu et al., 2016). These data are attractive for studying the channel capacity of chromatin regulation because the reporter gene was integrated site-specifically, used a strong promoter, and encoded for a highly stable protein product. This reduces the impact of genome positioning effects, noisy changes due to promoter state switching in the absence of targeting, and variation in protein degradation dynamics. Additionally, a large number of cells were profiled at each timepoint in the experiment, allowing for the fraction of active cells to be more precisely measured than would be possible with a significantly smaller population. Altogether, this meant that variation in the measured fraction of active cells was much more likely to be due to noise intrinsic to the chromatin regulator itself, rather than variation due to the experimental setup. We chose to consider KRAB, which featured significant epigenetic memory, and HDAC4, which featured no detectable long-term memory; the experiments demonstrated that at a synthetic reporter gene in CHO cells, KRAB featured parameters $k_a = 0.31/\text{day}, k_s = 11/\text{day}$, and $k_i = 0.13/\text{day}$, while HDAC4 featured $k_a = 0.76/\text{day}, k_s = 8.6/\text{day}$, and $k_i = 0/\text{day}$.

Because the ability to distinguish between different lengths of recruitment by measuring the silent fraction of cells varies over time as cells reactivate, the channel capacity for a given chromatin regulator is a function of the recruitment duration (t), and changes throughout the release period (τ). For both single-cell and population-level measures of channel capacity, we treated each duration of recruitment as a separate input (Fig. 4B). For the single-cell channel capacity, we used the expression values of the reporter gene in individual cells, as measured by flow cytometry, as the output. For the population-level, we used the fraction of cells with the reporter silenced as the output. Since for the population-level the number of experimental replicates was limited, we used bootstrapping to build input–output joint probability distributions and compute channel capacities (Supplementary Information). We computed the channel capacity throughout the first 15 days after CR release for both KRAB and HDAC4 at the single-cell (Fig. 4C) and population level (Fig. 4D). The single-cell channel capacity rapidly decayed during reactivation, consistent with stochastic reactivation reducing the ability of any single cell to communicate whether or not it had been silenced by a chromatin regulator. The population-level channel capacity of KRAB remained steady throughout reactivation while the population-level channel capacity for HDAC4 rapidly fell during release, consistent with the fact that KRAB has significant long-term epigenetic memory while HDAC4 does not. Since the experiment was set up with 4 discrete input recruitment durations, the estimated population-level channel capacity can be no greater than 2, regardless of whether or not chromatin regulation permits signaling with higher fidelity. The observation that empirical channel capacities are lower at the single-cell level than at the population level matched previous measurements of information flow in the all-or-none apoptosis signaling pathway (Suderman et al., 2017).

In order to understand the channel capacity of a system in which CRs are recruited for arbitrary lengths of time, we switched to theoretical models (single-cell and population) featuring a fully continuous input domain. We modeled single-cell information flow via the Z-channel (Tallini et al., 2002), which consists of a binary input mapping to a binary output with some error probability

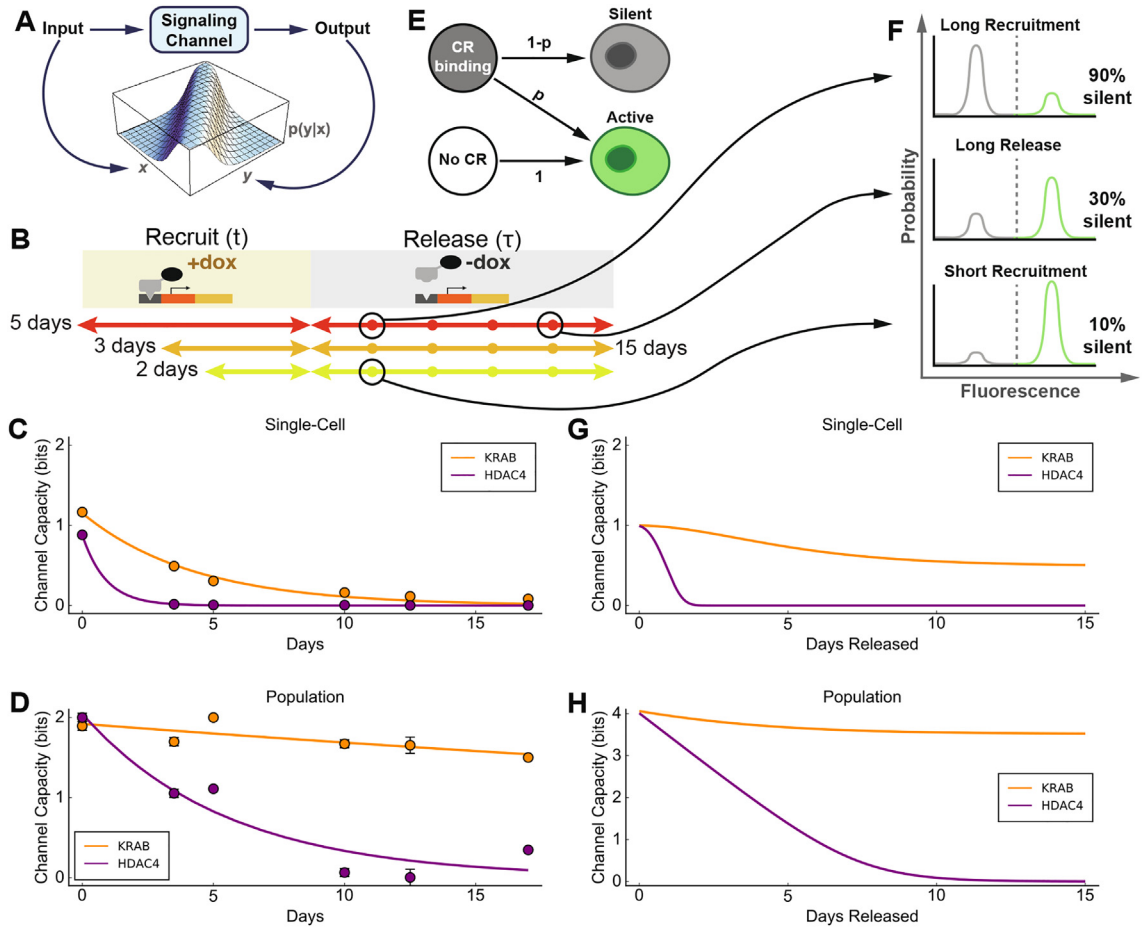

Fig. 4. Information-theoretic analysis of CR signaling capacities at the population versus single-cell level. A. Channel capacities measure the ability of a channel to transmit signals by determining how the distribution of inputs to the channel constrains the distribution of outputs from the channel. B. Experimental setup: Input recruitment periods are discrete: 0,2,3,5 days. Channel capacity is measured either at the very end of recruitment (0 days release), or at the indicated times after the CR was released (up to 15 days). C. Single-cell channel capacity as a function of time during the CR release period, computed using flow cytometry distributions for KRAB (CR with memory) and HDAC4 (CR without memory) using data from (Bintu et al., 2016). Recruitment was performed for 0, 2, 3, or 5 days and FITC values for individual cells were used to determine the channel capacity and its standard deviation (**Supplementary Information**). Curves represent exponential fits. D. Population channel capacity computed using the fraction of cells silenced for KRAB (CR with memory) and HDAC4 (CR without memory) using data from (Bintu et al., 2016). Recruitment was performed for 0, 2, 3, or 5 days. Error bars represent standard deviations of 3 independently calculated channel capacities (**Supplementary Information**). E. Single-cell information flow: Z-channel model for CR-mediated silencing. F. Population-level information encoded as the fraction of cells silent over time. G. Theoretical single-cell channel capacity of KRAB and HDAC4 as function of time after CR release using a Z-channel model for gene silencing upon CR recruitment. H. Theoretical population channel capacity of KRAB and HDAC4 as function of time after CR release, using an additive white Gaussian noise (AWGN) model with $\sigma = 0.0035$ (matching experimental noise magnitude).

(Fig. 4E). In this model, the input signal is whether or not a CR was recruited, while the output is the cell's promoter state: silent or active. For a Z-channel with error probability p, the channel capacity C can be shown to be (Supplementary Information §4.1, Tallini et al., 2002):

$$C = \log_2\left(1 + (1-p)p^{p/(1-p)}\right) \tag{3}$$

In this context, the error probability p refers to the probability that a cell is in the active state despite a repressive CR being recruited in that cell (Fig. 4E). This probability is equal to the fraction of active cells and depends on the durations of recruitment (t) and release (τ): $p(t,\tau) = A(t,\tau)$. Close to the beginning of release ($\tau \approx 0$), very few cells in the population will have stochastically reactivated ($p \approx 0$), and the silent state of a cell will properly reflect that the CR was recruited ($C \approx 1$).

For a CR with little to no memory such as HDAC4, towards the end of release ($\tau \gg 0$) most cells will have stochastically reactivated ($p = A(t,\tau) \approx 1$). As a result, the gene expression state of a cell will not accurately reflect CR recruitment and the channel capacity will decrease to 0 (Fig. 4G, HDAC4). Indeed, the empirical single-cell channel capacity for HDAC4 decreases after release to 0, matching these theoretical predictions (Fig. 4C).

In contrast, for a CR with significant long-term memory such as KRAB, even as the release time τ increases, many cells will not reactivate due to being irreversibly silenced ($p = A(t,\tau) < 1$). For these cells, their gene expression state will properly reflect CR recruitment, and as a result the channel capacity is not predicted to decrease all the way to 0 (Fig. 4G, KRAB). However, for KRAB the experimental measurements approach a channel capacity of 0 as time goes on (Fig. 4C). This is due to the presence of cells in the experimental data that silenced without CR recruitment; this background silencing is normalized out during computation of the rate constants for a given CR.

At the scale of a full population of cells, the ability of that population to encode the duration of recruitment via the fraction of silent cells is dependent on the number of cells and the noise in the system. At the scale of tens to hundreds of thousands of cells, as is the case in our experimental data, the limiting factor in the precision of this signaling is the noise, not the size of the popula-

tion. As a result, in order to model population-level information flow, we used an additive white Gaussian noise (AWGN) model (MacKay and Mac, 2003).

In this model, recruitment and release times were mapped to the idealized fraction cells silent predicted by the analytical solution of the 3-state model (Fig. 4F). After this, zero-mean Gaussian noise was added to the idealized fraction off to model the stochastically varying nature of the experimentally measured fraction of silent cells (Supplementary Information). Using the experimental data, we estimated the average variance in the experimentally measured fraction of silenced cells to be approximately 0.0035 for both KRAB and HDAC4, giving us an empirical estimate of the variance N for the zero-mean Gaussian noise.

The channel capacity for the AWGN model demonstrates that the ability of the system to transmit information depends on the ratio of the magnitude of the signal (called the power of the system, P) to the magnitude of the noise (N).

In particular, the channel capacity C can be computed as (Supplementary Information §4.2, MacKay and Mac, 2003):

$$C = \frac{1}{2}\log_2\left(1+\frac{P}{N}\right). \tag{4}$$

For this model featuring additive white Gaussian noise, the power P of the system can be thought of as the maximum possible magnitude of the fraction of silent cells. This is simply the fraction of cells predicted to be silent by the 3-state model for different durations of recruitment (t) and release (τ): $P = 1 - A(t,\tau)$.

During recruitment (t variable, and $\tau = 0$) the channel capacity for both KRAB and HDAC4 rose rapidly until plateauing at approximately 4 bits, consistent with both being fast silencers that can take advantage of the full dynamic range of population-level fractional silencing within a short period of time (Figure S3A).

Throughout release ($t = 5, \tau$ variable), the population channel capacity of KRAB remained relatively stable, while that of HDAC4 rapidly decreased to zero (Fig. 4H). Intuitively this happens because KRAB has long-term memory, while HDAC4's lack of epigenetic memory means that stochastic reactivation causes all cells to reactivate. Early on in release when many cells are silent and few have reactivated, the fraction of silent cells accurately reflects the duration of recruitment ($P = 1 - A(t,\tau) \gg 0$). As a result, the magnitude of the signal will be much greater than the magnitude of the noise ($P = 1 - A(t,\tau) \gg N$), and the channel capacity C at this stage will be relatively high. However, as time goes on, cells begin to reactivate, causing the fraction of silent cells to drop. As a result, the magnitude of the noise begins to overwhelm the magnitude of the signal ($P = 1 - A(t,\tau) \ll N$) and the channel capacity drops.

Using the experimental estimate of the output noise (0.0035), we computed theoretical channel capacities of approximately 4 bits for KRAB and HDAC4. These values are similar to the population-level channel capacity of the apoptosis signaling pathway in response to TRAIL, which was computed to be between 2.4 and 3.5 bits (Suderman et al., 2017). However, these values decrease sharply with increased output noise (i.e. random variation in the fraction of cells silenced by a stimulus) (Figure S3B) or input noise (i.e stochastic variation in the actual duration of CR recruitment in individual cells) (Figure S3C). These results are consistent with prior research demonstrating that the magnitude of noise in cell signaling pathways constrains information transmission (Cheong et al., 2011; Eldar and Elowitz, 2010; Selimkhanov et al., 2014; Suderman et al., 2017).

5. Discussion

In this paper we provide a theoretical framework for characterizing the behavior of genes regulated by chromatin regulators in response to temporal signals of different durations. We focused on chromatin regulators as molecular tools that can encode the duration of input signals as a fraction of cells in the population with the target gene active. This type of population-level fractional control of gene expression is enabled by stochastic all-or-none silencing at the level of single cells (Allshire and Madhani, 2018). While modulating the concentration of a chromatin regulator can change the specific rates associated with epigenetic silencing, reactivation, and memory, it does not change this fundamental property of chromatin regulators (Bintu et al., 2016).

Duration-dependent control can also be achieved via the accumulation of DNA mutations at a constant rate, such that the total number of mutations is proportional to the duration of a signal (Alemany et al., 2018; Frieda et al., 2017; McKenna et al., 2016; Park et al., 2021; Spanjaard et al., 2018; Tang and Liu, 2018). However, unlike memoryless repressive chromatin regulators, these alternative mechanisms are not easily reversible. Additionally, because each cell can accumulate multiple mutations to DNA, generating duration-dependent fractional control where certain cells do not feature any mutations may prove more challenging.

Classical transcription factors can use switch-like responses to input signal concentration to filter out noise (Tang and Liu, 2017; Thattai and van Oudenaarden, 2002). These responses are characterized by a non-responsive region at low input concentrations, followed by a regime of linearly increasing responses to input concentration, after which the response saturates. In contrast, the population-level responses to increasing durations of CR binding immediately increase linearly with the duration before they saturate. Nevertheless, even a single memoryless repressor CR can filter out high-frequency noise without the need for a complex signaling cascade. The precise level at which noise is filtered can be tuned by modulating the silencing and reactivation kinetics of the chromatin regulator; this can be done by changing the CR's concentration or binding site affinity, its localization, or the number of binding sites for the CR. Intriguingly, histone deacetylases, which are known to translocate into and out of the nucleus (Joshi et al., 2013), have been observed to be memoryless repressors in prior experiments (Bintu et al., 2016), suggesting that they may be ideal candidates for designing synthetic circuits that filter out such noise.

Autoregulatory loops with classical transcription factors can be used to speed up responses to stimuli and cap their own steady-state levels in individual cells (Alon, 2019). These loops can use promoters with different strengths to modulate the speed of the response in single cells (Rosenfeld et al., 2002), and can independently tune the steady-state value of the response by tuning the strength of binding or transcriptional activation. In regimes involving high rates of protein degradation, autoregulatory loops involving CRs can act similarly to classical transcription factors: they control the amount of CR present in active cells and how quickly individual cells converge to steady-state protein levels. However, unlike autoregulatory loops involving classical transcription factors, CR autoregulatory loops can also control the fraction of cells in a population that express a gene via the silencing and activation rates of the CR. While classical transcription factor autoregulatory loops produce populations with homogeneous output levels, autoregulatory CR loops produce heterogeneous populations with tunable fractions of cells at different expression levels.

Transcription factor circuits can also be used to measure signal duration, for example by precisely tuning degradation dynamics within positive feedback loops (Murphy et al., 2002) or by using coherent feedforward loops to generate all-or-none responses at the single-cell level (Mangan et al., 2003). However, input signals to transcription factor signaling networks more frequently manipulate the concentration of transcription factors via degradation (Chassin et al., 2019), competitive binding (Sokolik et al., 2015),

or translocation (Hao and O'Shea, 2012). In contrast, chromatin regulators with memory are able to encode the duration of temporal signals with ease and without the need for accumulations of external secondary products that must then be sensed by an external downstream signaling factor. This allows for the construction of compact temporal sensors that can both measure the total duration of chromatin regulator recruitment and produce adaptive responses to stimuli.

Similarly to autoregulatory loops, incoherent feedforward loops are among the most common gene network motifs. Incoherent feedforward loops generate pulse-like responses to increasing stimuli and allow for fold-change detection in biological circuits (Goentoro et al., 2009). We show that an incoherent feedforward loop consisting of chromatin repressors and activators can produce population pulses where a fraction of cells respond at full expression level for a limited period of time in response to a continuous signal. By manipulating the rates of silencing and reactivation associated with the chromatin regulators in the feedforward loop, we were able to tune both the magnitude and duration of this population pulse. In our incoherent loop the negative arm is controlled by a chromatin repressor with long-term epigenetic memory, so silenced cells are converted to an irreversibly silent state from which they can not respond to subsequent stimuli. This change in response is analogous to other instances of state-dependent inactivation used for generating perfect adaptation (Friedlander and Brenner, 2009), and allows for the construction of single-use epigenetic circuits that can only fire once. Such circuits could prove useful in scenarios including development, where genes need to be expressed at specific times (Nguyen et al., 2018), or immune regulation, where responses are reduced after chronic antigen exposure (Wherry and Kurachi, 2015). It is worth noting that our models involving repressor CRs that have long-term epigenetic memory do not incorporate the effects of noise or variability in the fraction of cells silenced on circuit behavior. However, in these scenarios involving small population sizes, it would be interesting to determine how noise affects the dynamic responses of gene circuits to temporal signals.

By analyzing chromatin regulation as an information-theoretic communication channel we are able to demonstrate that despite relatively low channel capacities at the single-cell level, the stochasticity of the single-cell response results in a high population-level channel capacity. We find that chromatin-dependent gene regulation features comparable channel capacities to apoptosis signaling, which also features binary single-cell and fractional population-level responses (Suderman et al., 2017). As has been demonstrated in prior theoretical models specific to transcription-factor mediated gene regulation, we find that levels of input and output noise constrain the channel capacity of chromatin regulators (Tkacik et al., 2008). These theoretical analyses of transcription factor signaling have found that physiologically reasonable choices for input noise, transcription factor concentration, and other biophysical parameters can produce channel capacities over 1 bit even in the context of a single gene responding to a single transcription factor (Tkačik et al., 2008; Tkačik et al., 2008). In contrast, because chromatin-mediated gene silencing is all-or-none, we observed that the single-cell channel capacity of chromatin regulators did not significantly exceed 1 bit.

Additionally, analyses of TNF signaling have shown that composing signaling pathways into more complex networks with positive and negative feedback can help reduce noisy signaling in both single cells and populations (Cheong et al., 2011). Characterizing such circuits in the context of chromatin regulation and analyzing the relationships between channel capacity, circuit architecture, and the concentration and binding of chromatin regulators will further elucidate how these biophysical parameters affect the channel capacity of chromatin regulation.

Recent work on gene regulation in *E. coli* experimentally validated predictions for the channel capacity of a simple genetic circuit using a minimal mechanistic model of transcriptional control in which all parameters were derived from published experimental datasets (Razo-Mejia et al., 2020). Such an analysis in mammalian cells would help explain how information is differentially encoded in TF and CR occupancy at genes, histone modifications, chromatin accessibility, 3D chromatin structure, and other potential determinants of gene expression. Major global efforts to exhaustively describe and experimentally measure all these parameters are underway.

CRediT authorship contribution statement

Adi Mukund: Conceptualization, Methodology, Software, Validation, Formal analysis, Investigation, Writing - original draft, Writing - review & editing. **Lacramioara Bintu:** Conceptualization, Methodology, Validation, Investigation, Resources, Supervision, Project administration, Funding acquisition.

Declaration of Competing Interest

The authors declare that they have no known competing financial interests or personal relationships that could have appeared to influence the work reported in this paper.

Acknowledgements

We thank Saba Eskandarian, Taihei Fujimori, Anton Geraschenko, Michaela Hinks, Stevan Jeknic, and Zeppelin Cat for helpful conversations and assistance. We thank members of the Bintu lab for helpful feedback. Figs. 2A and 3D were made with Biorender.com. This work was supported by BWF CASI (LB), NIH-NIGMS R35M128947 (LB), and training grant 5T32GM007365-45 (AM).

Appendix A. Supplementary data

Supplementary data associated with this article can be found, in the online version, at https://doi.org/10.1016/j.jtbi.2021.110977. Code related to this manuscript is available at https://github.com/bintulab/cr_theory_mukund2021.

References

Alemany, A., Florescu, M., Baron, C.S., Peterson-Maduro, J., van Oudenaarden, A., 2018. Whole-organism clone tracing using single-cell sequencing. Nature 556 (7699), 108–112. https://doi.org/10.1038/nature25969.

Allis, C.D., Jenuwein, T., 2016. The molecular hallmarks of epigenetic control, Nature reviews. Genetics 17 (8), 487–500. https://doi.org/10.1038/nrg.2016.59.

Allshire, R.C., Madhani, H.D., 2018. Ten principles of heterochromatin formation and function, Nature reviews. Mol. Cell Biology 19 (4), 229–244. https://doi.org/10.1038/nrm.2017.119.

Alon, U., 2019. An Introduction to Systems Biology: Design Principles of Biological Circuits. CRC Press.

M.A. Al-Radhawi, M. Ali Al-Radhawi, D. Del Vecchio, E.D. Sontag, Multi-modality in gene regulatory networks with slow promoter kinetics (2019). doi:10.1371/journal.pcbi.1006784..

Amabile, A., Migliara, A., Capasso, P., Biffi, M., Cittaro, D., Naldini, L., Lombardo, A., 2016. Inheritable silencing of endogenous genes by Hit-and-Run targeted epigenetic editing. Cell 167 (1), 219–232.e14. https://doi.org/10.1016/j.cell.2016.09.006.

Badeaux, A.I., Shi, Y., 2013. Emerging roles for chromatin as a signal integration and storage platform, Nature reviews. Mol. Cell Biol. 14 (4), 211–224. https://doi.org/10.1038/nrm3545.

Bintu, L., Buchler, N.E., Garcia, H.G., Gerland, U., Hwa, T., Kondev, J., Phillips, R., 2005. Transcriptional regulation by the numbers: Models. Current Opinion Genetics Dev. 15 (2), 116–124. https://doi.org/10.1016/j.gde.2005.02.007.

Bintu, L., Yong, J., Antebi, Y.E., McCue, K., Kazuki, Y., Uno, N., Oshimura, M., Elowitz, M.B., 2016. Dynamics of epigenetic regulation at the single-cell level. Science 351 (6274), 720–724. https://doi.org/10.1126/science.aab2956.

Bleris, L., Xie, Z., Glass, D., Adadey, A., Sontag, E., Benenson, Y., 2011. Synthetic incoherent feedforward circuits show adaptation to the amount of their genetic template. Mol. Syst. Biol. 7, 519. https://doi.org/10.1038/msb.2011.49.

Chassin, H., Müller, M., Tigges, M., Scheller, L., Lang, M., Fussenegger, M., 2019. A modular degron library for synthetic circuits in mammalian cells. Nature Commun. 10 (1), 2013. https://doi.org/10.1038/s41467-019-09974-5.

Chen, T., Dent, S.Y.R., 2014. Chromatin modifiers and remodellers: regulators of cellular differentiation, Nature reviews. Genetics 15 (2), 93–106. https://doi.org/10.1038/nrg3607.

Cheong, R., Rhee, A., Wang, C.J., Nemenman, I., Levchenko, A., 2011. Information transduction capacity of noisy biochemical signaling networks. Science 6054 (October), 354–358.

Crews, S.T., Pearson, J.C., 2009. Transcriptional autoregulation in development. Current Biol.: CB 19 (6), R241–6. https://doi.org/10.1016/j.cub.2009.01.015.

Dalal, C.K., Cai, L., Lin, Y., Rahbar, K., Elowitz, M.B., 2014. Pulsatile dynamics in the yeast proteome. Current Biol.: CB 24 (18), 2189–2194. https://doi.org/10.1016/j.cub.2014.07.076.

Doherty, M.K., Hammond, D.E., Clague, M.J., Gaskell, S.J., Beynon, R.J., 2009. Turnover of the human proteome: determination of protein intracellular stability by dynamic SILAC. J. Proteome Res. 8 (1), 104–112. https://doi.org/10.1021/pr800641v.

Eldar, A., Elowitz, M.B., 2010. Functional roles for noise in genetic circuits. Nature 467 (7312), 167–173. https://doi.org/10.1038/nature09326.

Ferrell, J.E., 2016. Perfect and near-perfect adaptation in cell signaling. Cell Syst. 2 (2), 62–67. https://doi.org/10.1016/j.cels.2016.02.006.

Ferrell Jr, J.E., Machleder, E.M., 1998. The biochemical basis of an all-or-none cell fate switch in xenopus oocytes. Science 280 (5365), 895–898. https://doi.org/10.1126/science.280.5365.895.

Fraser, D., Kaern, M., 2009. A chance at survival: gene expression noise and phenotypic diversification strategies. Mol. Microbiol. 71 (6), 1333–1340. https://doi.org/10.1111/j.1365-2958.2009.06605.x.

Frieda, K.L., Linton, J.M., Hormoz, S., Choi, J., Chow, K.H.K., Singer, Z.S., Budde, M.W., Elowitz, M.B., Cai, L., 2017. Synthetic recording and in situ readout of lineage information in single cells. Nature 541 (7635), 107–111. https://doi.org/10.1038/nature20777.

Friedlander, T., Brenner, N., 2009. Adaptive response by state-dependent inactivation. Proc. National Acad. Sci. USA 106 (52), 22558–22563. https://doi.org/10.1073/pnas.0902146106.

Garcia, H.G., Phillips, R., 2011. Quantitative dissection of the simple repression input-output function. Proc. National Acad. Sci. USA 108 (29), 12173–12178. https://doi.org/10.1073/pnas.1015616108.

Garcia, H.G., Sanchez, A., Kuhlman, T., Kondev, J., Phillips, R., 2010. Transcription by the numbers redux: experiments and calculations that surprise. Trends Cell Biology 20 (12), 723–733. https://doi.org/10.1016/j.tcb.2010.07.002.

Gil, J., O'Loghlen, A., 2014. PRC1 complex diversity: where is it taking us? Trends Cell Biol. 24 (11), 632–641. https://doi.org/10.1016/j.tcb.2014.06.005.

Goentoro, L., Shoval, O., Kirschner, M.W., Alon, U., 2009. The incoherent feedforward loop can provide fold-change detection in gene regulation. Molecular cell 36 (5), 894–899. https://doi.org/10.1016/j.molcel.2009.11.018.

Hao, N., O'Shea, E.K., 2012. Signal-dependent dynamics of transcription factor translocation controls gene expression. Nature Struct. Mol. Biol. 19 (1), 31–40. https://doi.org/10.1038/nsmb.2192.

Hathaway, N.A., Bell, O., Hodges, C., Miller, E.L., Neel, D.S., Crabtree, G.R., 2012. Dynamics and memory of heterochromatin in living cells. Cell 149 (7), 1447–1460. https://doi.org/10.1016/j.cell.2012.03.052.

Husmann, D., Gozani, O., 2019. Histone lysine methyltransferases in biology and disease. Nature Struct. Mol. Biol. 26 (10), 880–889. https://doi.org/10.1038/s41594-019-0298-7.

Joshi, P., Greco, T.M., Guise, A.J., Luo, Y., Yu, F., Nesvizhskii, A.I., Cristea, I.M., 2013. The functional interactome landscape of the human histone deacetylase family. Mol. Syst. Biol. 9, 672. https://doi.org/10.1038/msb.2013.26.

Komorowski, M., Tawfik, D.S., 2019. The limited information capacity of Cross-Reactive sensors drives the evolutionary expansion of signaling. Cell Syst. 8 (1), 76–85.e6. https://doi.org/10.1016/j.cels.2018.12.006.

J.B. Lee, L.M. Caywood, J.Y. Lo, N. Levering, A.J. Keung, Mapping the dynamic transfer functions of eukaryotic gene regulation, Cell Systems doi:10.1016/j.cels.2021.08.003. URL:https://www.sciencedirect.com/science/article/pii/S240547122100291X..

Levine, J.H., Fontes, M.E., Dworkin, J., Elowitz, M.B., 2012. Pulsed feedback defers cellular differentiation. PLoS Biol. 10, (1). https://doi.org/10.1371/journal.pbio.1001252 e1001252.

Levine, J.H., Lin, Y., Elowitz, M.B., 2013. Functional roles of pulsing in genetic circuits. Science 342 (6163), 1193–1200. https://doi.org/10.1126/science.1239999.

Lin, Y., Sohn, C.H., Dalal, C.K., Cai, L., Elowitz, M.B., 2015. Combinatorial gene regulation by modulation of relative pulse timing. Nature 527 (7576), 54–58. https://doi.org/10.1038/nature15710.

MacKay, D.J.C., Mac, D.J., 2003. Information Theory, Inference and Learning Algorithms. Cambridge University Press.

Y. Ma, M.W. vxudde, M.N. Mayalu, J. Zhu, R.M. Murray, M.B. Elowitz, Synthetic mammalian signaling circuits for robust cell population control, available online at https://www.biorxiv.org/content/early/2020/09/03/2020.09.02.278564 (Sep. 2020). arXiv:https://www.biorxiv.org/content/early/2020/09/03/2020.09.02.278564.full.pdf, doi:10.1101/2020.09.02.278564. URL: https://www.biorxiv.org/content/early/2020/09/03/2020.09.02.278564..

Mangan, S., Zaslaver, A., Alon, U., 2003. The coherent feedforward loop serves as a sign-sensitive delay element in transcription networks. J. Mol. Biol. 334 (2), 197–204. https://doi.org/10.1016/j.jmb.2003.09.049.

McKenna, A., Findlay, G.M., Gagnon, J.A., Horwitz, M.S., Schier, A.F., Shendure, J., 2016. Whole-organism lineage tracing by combinatorial and cumulative genome editing. Science 353 (6298), aaf7907. https://doi.org/10.1126/science.aaf7907.

Murphy, L.O., Smith, S., Chen, R.-H., Fingar, D.C., Blenis, J., 2002. Molecular interpretation of ERK signal duration by immediate early gene products. Nature Cell Biol. 4 (8), 556–564. https://doi.org/10.1038/ncb822.

Ng, H.H., Bird, A., 2000. Histone deacetylases: silencers for hire. Trends Biochemical Sci. 25 (3), 121–126. https://doi.org/10.1016/s0968-0004(00)01551-6.

K.K. Ng, M.A. Yui, A. Mehta, S. Siu, B. Irwin, S. Pease, S. Hirose, M.B. Elowitz, E.V. Rothenberg, H.Y. Kueh, A stochastic epigenetic switch controls the dynamics of t-cell lineage commitment, eLife 7. doi:10.7554/eLife.37851..

Nguyen, H., Kerimoglu, C., Pirouz, M., Pham, L., Kiszka, K.A., Sokpor, G., Sakib, M.S., Rosenbusch, J., Teichmann, U., Seong, R.H., Stoykova, A., Fischer, A., Staiger, J.F., Tuoc, T., 2018. Epigenetic regulation by BAF complexes limits neural stem cell proliferation by suppressing wnt signaling in late embryonic development. Stem Cell Rep. 10 (6), 1734–1750. https://doi.org/10.1016/j.stemcr.2018.04.014.

Ochab-Marcinek, A., Jędrak, J., Tabaka, M., 2017. Hill kinetics as a noise filter: the role of transcription factor autoregulation in gene cascades. Phys. Chem. Chem. Phys.: PCCP 19 (33), 22580–22591. https://doi.org/10.1039/c7cp00743d.

Park, J., Lim, J.M., Jung, I., Heo, S.-J., Park, J., Chang, Y., Kim, H.K., Jung, D., Yu, J.H., Min, S., Yoon, S., Cho, S.-R., Park, T., Kim, H.H., 2021. Recording of elapsed time and temporal information about biological events using cas9. Cell 184 (4), 1047–1063.e23. https://doi.org/10.1016/j.cell.2021.01.014.

Razo-Mejia, M., Marzen, S., Chure, G., Taubman, R., Morrison, M., Phillips, R., 2020. First-principles prediction of the information processing capacity of a simple genetic circuit. Phys. Rev. E 102, (2). https://doi.org/10.1103/PhysRevE.102.022404 022404.

Rosenfeld, N., Elowitz, M.B., Alon, U., 2002. Negative autoregulation speeds the response times of transcription networks. J. Mol. Biol. 323 (5), 785–793. https://doi.org/10.1016/s0022-2836(02)00994-4.

Sasse, S.K., Gerber, A.N., 2015. Feed-forward transcriptional programming by nuclear receptors: regulatory principles and therapeutic implications. Pharmacol. Therapeutics 145, 85–91. https://doi.org/10.1016/j.pharmthera.2014.08.004.

Selimkhanov, J., Taylor, B., Yao, J., Pilko, A., Albeck, J., Hoffmann, A., Tsimring, L., Wollman, R., 2014. Accurate information transmission through dynamic biochemical signaling networks. Science 346 (6215), 1370–1373. https://doi.org/10.1126/science.1254933.

Shaffer, S.M., Dunagin, M.C., Torborg, S.R., Torre, E.A., Emert, B., Krepler, C., Beqiri, M., Sproesser, K., Brafford, P.A., Xiao, M., Eggan, E., Anastopoulos, I.N., Vargas-Garcia, C.A., Singh, A., Nathanson, K.L., Herlyn, M., Raj, A., 2017. Rare cell variability and drug-induced reprogramming as a mode of cancer drug resistance. Nature 546 (7658), 431–435. https://doi.org/10.1038/nature22794.

C.E. Shannon, A mathematical theory of communication, Bell System Technical Journal 27 (April 1928) (1948) 379–423,623–656..

Sokolik, C., Liu, Y., Bauer, D., McPherson, J., Broeker, M., Heimberg, G., Qi, L.S., Sivak, D.A., Thomson, M., 2015. Transcription factor competition allows embryonic stem cells to distinguish authentic signals from noise. Cell Syst. 1 (2), 117–129. https://doi.org/10.1016/j.cels.2015.08.001.

Song, J., Angel, A., Howard, M., Dean, C., 2012. Vernalization - a cold-induced epigenetic switch. J. Cell Sci. 125 (Pt 16), 3723–3731. https://doi.org/10.1242/jcs.084764.

Spanjaard, B., Hu, B., Mitic, N., Olivares-Chauvet, P., Janjuha, S., Ninov, N., Junker, J.P., 2018. Simultaneous lineage tracing and cell-type identification using CRISPR–Cas9-induced genetic scars. Nature Biotechnol. 36 (5), 469–473. https://doi.org/10.1038/nbt.4124.

Suderman, R., Bachman, J.A., Smith, A., Sorger, P.K., Deeds, E.J., 2017. Fundamental trade-offs between information flow in single cells and cellular populations. Proc. Nat. Acad. Sci. 114 (22), 5755–5760. https://doi.org/10.1073/pnas.1615660114.

Tallini, L.G., Al-Bassam, S., Bose, B., 2002. On the capacity and codes for the z-channel, in. In: Proceedings IEEE International Symposium on Information Theory, p. 422. https://doi.org/10.1109/ISIT.2002.1023694.

W. Tang, D.R. Liu, Rewritable multi-event analog recording in bacterial and mammalian cells (2018). doi:10.1126/science.aap8992..

Tay, S., Hughey, J.J., Lee, T.K., Lipniacki, T., Quake, S.R., Covert, M.W., 2010. Single-cell NF-B dynamics reveal digital activation and analogue information processing. Nature 466 (7303), 267–271. https://doi.org/10.1038/nature09145.

P.I. Thakore, J.B. Black, I.B. Hilton, C.A. Gersbach, Editing the epigenome: technologies for programmable transcription and epigenetic modulation (2016). doi:10.1038/nmeth.3733..

Thattai, M., van Oudenaarden, A., 2002. Attenuation of noise in ultrasensitive signaling cascades. Biophys. J. 82 (6), 2943–2950. https://doi.org/10.1016/S0006-3495(02)75635-X.

Tkacik, G., Gregor, T., Bialek, W., 2008. The role of input noise in transcriptional regulation. PloS one 3, (7). https://doi.org/10.1371/journal.pone.0002774 e2774.

Tkačik, G., Callan, C.G., Bialek, W., 2008. Information capacity of genetic regulatory elements. Phys. Rev. E 78, (1). https://doi.org/10.1103/PhysRevE.78.011910 011910.

Tkačik, G., Callan, C.G., Bialek, W., 2008. Information flow and optimization in transcriptional regulation. Proc. National Acad. Sci. USA 105 (34), 12265–12270. https://doi.org/10.1073/pnas.0806077105.

Uda, S., Kuroda, S., 2016. Analysis of cellular signal transduction from an information theoretic approach. Seminars Cell Dev. Biol. 51, 24–31. https://doi.org/10.1016/j.semcdb.2015.12.011.

Uda, S., Saito, T.H., Kudo, T., Kokaji, T., Tsuchiya, T., Kubota, H., Komori, Y., Ozaki, Y.-I., Kuroda, S., 2013. Robustness and compensation of information transmission of signaling pathways. Science 341 (6145), 558–561. https://doi.org/10.1126/science.1234511.

Valencia, A.M., Kadoch, C., 2019. Chromatin regulatory mechanisms and therapeutic opportunities in cancer. Nature Cell Biol. 21 (2), 152–161. https://doi.org/10.1038/s41556-018-0258-1.

Wertek, F., Xu, C., 2014. Digital response in T cells: to be or not to be. Cell research 24 (3), 265–266. https://doi.org/10.1038/cr.2014.5.

Wherry, E.J., Kurachi, M., 2015. Molecular and cellular insights into T cell exhaustion, Nature reviews. Immunology 15 (8), 486–499. https://doi.org/10.1038/nri3862.